Magnetic-Responsive Release Controlled by Hot Spot Effect

Eduardo Guisasola,[†] Alejandro Baeza,[†] Marina Talelli,[†] Daniel Arcos,[†] María Moros,[‡,⊥] Jesús M. de la Fuente,[§] and María Vallet-Regí*[,†]

[†]Departamento de Química Inorgánica y Bioinorgánica, UCM, Instituto de Investigación Sanitaria Hospital 12 de Octubre i+12, Centro de Investigación Biomédica en Red de Bioingeniería, Biomateriales y Nanomedicina (CIBER-BBN), 28029 Madrid, Spain

[‡]Instituto de Nanociencia de Aragon, Universidad de Zaragoza, C/Mariano Esquillor s/n, 50018 Zaragoza, Spain

[⊥]Istituto di Scienze Applicate e Sistemi Intelligenti "Eduardo Caianiello", Via Campi Flegrei 34, 80078 Pozzuoli (Naples), Italy

[§]Instituto de Ciencia de Materiales de Aragón, CSIC-Universidad de Zaragoza, C/Pedro Cerbuna 12, 50018 Zaragoza, Spain

ABSTRACT: Magnetically triggered drug delivery nanodevices have attracted great attention in nanomedicine, as they can feature as smart carriers releasing their payload at clinician's will. The key principle of these devices is based on the properties of magnetic cores to generate thermal energy in the presence of an alternating magnetic field. Then, the temperature increase triggers the drug release. Despite this potential, the rapid heat dissipation in living tissues is a serious hindrance for their clinical application. It is hypothesized that magnetic cores could act as hot spots, this is, produce enough heat to trigger the release without the necessity to increase the global temperature. Herein, a nanocarrier has been designed to respond when the temperature reaches 43 °C. This material has been able to release its payload under an alternating magnetic field without the need of increasing the global temperature of the environment, proving the efficacy of the hot spot mechanism in magnetic-responsive drug delivery devices.

INTRODUCTION

The design of new stimuli-responsive nanodevices is an ever-evolving research field for the development of efficient drug delivery systems, mainly for those addressed to the treatment of malignant diseases.[1] In the case of porous inorganic materials, their performance relays on the open−close response of nanogates commonly assembled at the pore entrance, which act as gatekeepers. In this sense, silica mesoporous nanoparticles have been widely demonstrated to be an excellent support for stimuli-responsive purposes.[2,3] Moreover, there is a range of sizes in which they are able to extend the blood circulation time. The consequence is an enhanced accumulation in tumor areas, through the enhanced permeation and retention effect[4] (EPR), allowing for more efficient and accurate treatments with fewer side effects.[5] After accumulation in the desired area, a stimuli responsive release is often desirable. For that purpose many stimuli have been used to trigger the cargo release such as pH,[6,7] light,[8] redox,[9] and others.[10,11] Among them, significant efforts have been made to develop magnetic-responsive nanodevices, which respond to noninvasive and highly penetrating alternating magnetic fields (AMF), inducing local heating by means of the magnetic losses of the nanoparticles.[12] Promising candidates in this field are magnetic mesoporous silica nanoparticles (MMSNPs) coated with thermosensitive polymers as a stimuli-responsive gating system.[13−15] However, magnetically induced heating systems undergo the serious inconvenience of their thermal dissipation by the bloodstream. Actually, their stimuli-responsive behavior strongly depends on the environmental heating, which is difficult to maintain while the blood irrigation increases.[16,17]

Recently, the local heating developed by magnetic nanoparticles has been tested using a DNA thermal probe[18] or an azo-functionalized polymer by thermal decomposition.[19] These works have demonstrated that the temperature reached by the magnetic nanoparticles is significantly higher than that measured in the surrounding media. Recently, Zink and co-workers[20] have also demonstrated that it is possible to reach an effective heating in the surface of silica nanoparticles in response to an alternating magnetic field due to embedded magnetite nanoparticles. These findings have opened the possibility for designing new stimuli-responsive devices that work on the basis of the *hot spot* effect. In other words, these systems would magnetically trigger the drug release, without the obligation of supplying high magnetic energies commonly required for heating the environment, thus overcoming the blood-mediated thermal dissipation. For this goal, the mesoporous silica surface was coated with an engineered thermosensitive random copolymer which exhibits a linear (soluble) to globular (insoluble) transition at 40−43 °C. Therefore, in physiological temperature, the polymer chains are extended and soluble, blocking the release, while above the transition temperature the polymer shrinks, allowing the cargo

 © XXXX American Chemical Society

release. The arch stone for this performance is the hot spots formed by the superparamagnetic iron oxide nanoparticles (SPION) embedded in the mesoporous silica matrix in response to an alternate magnetic field. This hot spot effect is shown to be capable to reach the polymer coating that blocks the mesopores, thus provoking the shrinkage of the polymer network and the release of its cargo.

The colloidal stability of nanocarriers is crucial for biomedical applications, especially in the case of intravenous administration.[21] Mesoporous silica nanoparticles have been widely studied as drug delivery vehicles but they often suffer from aggregation in the bloodstream, which could be solved by polymer attachment on the silica surface.[22] Coating of nanoparticles with poly(ethylene glycol) or other hydrophilic polymers is known to improve their colloidal stability in physiological conditions and increase their circulation times.[23] Therefore, we have developed a procedure for synthesis of magnetic mesoporous silica nanoparticles based on the key steps shown in Scheme 1.

Scheme 1. Synthesis Path of MMSNP@P(NIPAM/NHMA) Device

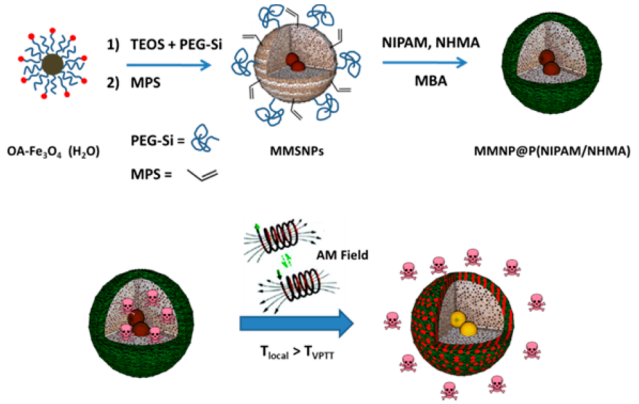

EXPERIMENTAL SECTION

Reagents. All chemicals were used without further purification. Tetraethyl orthosilicate (TEOS, 98%), *n*-cetyltrimethylammonium bromide (CTAB, 99%), 3-[tris(trimethylsiloxy)silyl]propyl methacrylate (TMSPMA, 98%), *N*-isopropylacrylamide (NIPAM, ≥99%), *N*-(hydroxymethyl)acrylamide solution (NHMA, 48 wt % in H_2O), *N*,*N*′-methylenebis(acrylamide) (MBA, 99%), oleic acid (OA, ≥99%), 4,4′-azobis(4-cyanovaleric acid) (ABCVA, ≥98.0%), fluorescein sodium salt, iron(II) chloride tetrahydrate ($FeCl_2{\cdot}4H_2O$, 99%), and iron(III) chloride hexahydrate ($FeCl_3{\cdot}6H_2O$, >99%) were obtained from Sigma-Aldrich. [Hydroxy(polyethyleneoxy)propyl] triethoxysilane, (PEG-Si, MW = 575−750 g/mol, 50% in ethanol) was purchased from Gelest. Ammonium nitrate (NH_4NO_3, 99.9%), ammonium hydroxide (NH_4OH, 28−30 wt % as NH_3), chloroform ($CHCl_3$, 99.8%), sodium hydroxide (NaOH, ≥98%), and absolute ethanol were purchased from Panreac. Ultrapure water was generated using a Millipore Milli-Q system with a Milli-pak filter of 0.22-μm pore size and used for the preparation of all aqueous solutions.

Characterization Techniques. Fourier transform infrared spectroscopy (FTIR) was performed in a Thermo Nicolet nexus equipped with a Goldengate attenuated total reflectance device. The textural properties of the materials were determined by nitrogen sorption porosimetry by using a Micromeritics ASAP 2020. To perform the N_2 measurements, the samples were previously degassed under vacuum for 24 h at room temperature. Thermogravimetry analysis (TGA) were performed in a Perkin Elmer Pyris Diamond TG/DTA analyzer, with 5 °C min^{-1} heating ramps, from room temperature to 600 °C. The hydrodynamic size of mesoporous and oleic acid iron oxide nanoparticles was measured by means of a Zetasizer Nano ZS (Malvern Instruments) equipped with a 633-nm "red" laser. Transmission electron microscopy (TEM) was carried out with a JEOL JEM 2100 instrument operated at 200 kV, equipped with a CCD camera (KeenView Camera). Sample preparation was performed by dispersion in distilled water and subsequent deposition onto carbon-coated copper grids. A solution of 1% of phosphotungstic acid (PTA) pH 7.0 was employed as staining agent in order to visualize the polymer coating attached on the mesoporous surface. Scanning electron microscopy (SEM) analyses were made on a JEOL 7600-LINK AN10000 microscope (Electron Microscopy Centre, UCM) using a graphite sample holder without any treatment. Liquid ^1H NMR experiments were made in a Bruker AV 250 MHz. UV−vis spectrometry was used to determine the LCST of linear polymers by means of a Biotek Synergy 4 device. Iron quantification for specific absorption rate (SAR) measurements at 480 nm absorbance was carried out on a Thermo Scientific Multiskan GO UV/vis microplate spectrophotometer. A calibration curve was performed following the same procedure using iron standard solution (Acros Organics) as reference. For DC magnetic field, magnetic parameters were determined by means of a vibrating sample magnetometer (VSM, Instituto de Sistemas Optoelectrónicos y Microtecnología, Universidad Politécnica de Madrid, Spain). Measurements were carried out at room temperature and applying a maximum DC field of 5000 G. The AMF assays were performed on a DM100 system (nanoScale Biomagnetics) in the frequency range from 424 to 838 kHz and magnetic fields of 20.05 to 23.87 kA·m^{-1}.

Calculation Procedures. The surface area was determined using the Brunauer−Emmett−Teller (BET) method, and the pore volume, V_{pore} (cm^3 g^{-1}), was estimated from the amount of N_2 adsorbed at a relative pressure around 0.99. The pore size distribution between 0.5 and 40 nm was calculated from the desorption branch of the isotherm by means of the Barrett−Joyner−Halenda (BJH) method. The mesopore size, $Ø_{pore}$ (nm), was determined from the maximum of the pore size distribution curve. The SAR calculations were performed by DM100 system software (nanoScale Biomagnetics). The mole percentage of NHMA (f_{NHMA}) in the synthesized random copolymers was determined using ^1H NMR analysis using eq 1. $I_{4.66\ ppm}$ and $I_{3.87\ ppm}$ are the integrals of the protons at 4.66 and 3.87 ppm, respectively.

$$f_{NHMA}\,(\%) = \frac{I_{4.66ppm}/2}{I_{3.87ppm} + I_{4.66ppm}/2} \times 100 \qquad (1)$$

Preparation of Hydrophobic Magnetite (Fe_3O_4) NPs. Hydrophobic magnetite NPs were synthesized by one-pot chemical coprecipitation method. Deionized water was purged with nitrogen gas for 10 min. Then 4.80 g of $FeCl_3{\cdot}6H_2O$, 2.00 g of $FeCl_2{\cdot}4H_2O$, and 0.85 mL of oleic acid were added to 30 mL of deionized water under nitrogen atmosphere with vigorous stirring. The mixture solution was heated to 90 °C. Then 20 mL of ammonium hydroxide (14 wt %) was added rapidly to the solution, and it immediately turned black. The reaction was kept at 90 °C for 2.5 h and then allowed to cool to room temperature. The black precipitate was collected by magnetic decantation and resuspended in chloroform with an end concentration of 32.8 mg·mL^{-1} oleic acid-capped Fe_3O_4.

Preparation of Mesoporous Magnetic Silica Nanoparticles (MMSNPs). MMSNPs were prepared in a 50-mL round-bottom flask, adding 582 mg of CTAB as a phase transfer agent and structure-directing agent for silica condensation that was dissolved in 10 mL of H_2O (mQ). The mixture was then mechanically stirred in an ultrasound bath during the addition of 26.4 mg of OA-Fe_3O_4 in $CHCl_3$ (0.04 mL·min^{-1} rate) until the complete removal of the organic solvent. The aqueous suspension was added through a 0.2-μm cellulose filter to an 86-mL NaOH (0.016M) solution and stirred at 600 rpm. When the suspension was stabilized at 45 °C, a mixture of 1.2 mL of EtOH and 1 mL of TEOS was added dropwise (0.25 mL·min^{-1} rate). Once the TEOS addition was finished, 130 μL of PEG-Si was added, and the suspension was stirred for 2 h. The reaction

mixture was washed three times by centrifugation with 50 mL of H_2O, and then two more times with 50 mL of EtOH. The brown solid obtained was suspended in 200 mL of EtOH (99.5%). Then, 0.5 mL of MPS was added dropwise and the mix was kept stirring at 40 °C during 16 h. Before the washing step with absolute EtOH, the surfactant template was removed by ion exchange using 175 mL of 10 $g{\cdot}L^{-1}$ NH_4NO_3 in EtOH (95%) extracting solution at 65 °C overnight. The brown suspension was then centrifuged (15 000 rpm, 30 min) and washed three times with 50 mL of EtOH to be dried under vacuum overnight.

Linear Polymers Synthesis. In a typical synthesis for a polymer with a 90:10 NIPAM to NHMA ratio, 200 mg (1.76 mmol) of NIPAM and 44.8 μL (0.19 mmol) of NHMA were placed in vial A and 12.7 mg of initiator 4,4′-azobis(4-cyanovaleric acid) (ABCVA) was placed in vial B. The monomer mixture and the initiator were purged by nitrogen flow prior to the addition of 2.5 and 1 mL of dry DMF, respectively, to each vial. The solutions were bubbled with N_2 for 15 min. Vial A was stirred in a heated oilbath at 80 °C for 2 min before the fast addition of 100 μL of vial B solution (1.2 mg, 400:1 monomer to initiator ratio), and allowed to stir for 16 h. A maximum 2 mL of the reaction mixture was added dropwise to 45 mL of EtO_2 in a centrifugation tube, obtaining a white precipitate. The precipitate was washed three times with 45 mL of diethyl ether and dried at ambient temperature. The white solid was dissolved in H_2O and lyophilized.

MMSNPs Polymer Coating. In a 100-mL three-neck round-bottom flask, 150.9 mg (1.33 mmol) of NIPAM, 12 mg of MBA (0.078 mmol), 49.4 μL of NHMA (0.148 mmol), 3.6 mg of CTAB, and 5 mg of Na_2CO_3 were added to 45 mL of water (mQ). The solution was stirred under N_2 bubbling at 70 °C for 30 min to remove oxygen. The solution was kept under N_2 and then 50 mg of MMSNPs redispersed in 5 mL of EtOH (99.5%) was added to the monomer solution and stirred for 15 min more. To initiate the monomer polymerization, 0.2 mL of a 25 $mg{\cdot}mL^{-1}$ APS solution in H_2O (mQ) previously deoxygenated was added to the reaction mixture. Twenty min after the initiator addition a brown solid precipitate appeared.The reaction mixture was allowed to cool to room temperature and kept at that temperature for 6 h. The mixture was centrifuged and washed three times with H_2O to remove the unreacted monomers and dried under vacuum overnight.

Fluorescein Release Experiments. Hybrid MMSN@P(NIPAM/NHMA) nanoparticles were loaded with a 20 $mg{\cdot}mL^{-1}$ fluorescein sodium salt solution in PBS (1×) at 50 °C for 16 h. The hybrid material was then washed with PBS (1×) until no fluorescence was observed. Fluorescein release experiments were carried out with 10 mg of fluorescein-loaded MMSN@P(NIPAM/NHMA) dispersed in 1 mL of PBS (1×) and divided into two 0.5-mL aliquots. To determine the polymer VPTT attached to the silica surface, one aliquot was submitted to a heating ramp in an incubator to the three target temperatures (37, 40, and 43 °C). The second aliquot was carried to an AC magnetic inductor to apply an 838 kHz and 20.05 $kA{\cdot}m^{-1}$ alternating magnetic field. The temperature increase developed by the nanoparticles was recorded with a fiber-optic probe. After the dispersion reached the target temperature, the samples were cooled and collected by centrifugation, and the fluorescence of supernatants was measured. Isotherm fluorescein release experiment was made by keeping one of the aliquots placed in the AC magnetic inductor under isotherm conditions at 37 °C with a water recirculating system. The other aliquot was kept at 37 °C in an incubator as control. Alternating magnetic field was applied. After 45 min the samples were cooled to 4 °C and collected by centrifugation, and the fluorescence of supernatants was measured.

RESULTS AND DISCUSSION

Ultrastable hydrophobic oleic acid iron oxide nanocrystals (OA-Fe_3O_4) were obtained by the coprecipitation method previously described by Haynes and colleagues,[24] obtaining a colloidal suspension in organic solvent of nanoparticles that present a diameter distribution centered on 6 nm, confirmed by TEM images (Supporting Information Figure S1). These magnetic cores were then transferred to an aqueous phase using *n*-cetyltrimethylammonium bromide (CTAB) solution, which acts as a phase transfer agent and as porous structure-directing agent at the same time. Next, a mesoporous silica matrix was formed by the slow addition of tetraethyl orthosilicate (TEOS) in the presence of NaOH as a catalyst. After the addition of TEOS, a solution of sililated poly(ethylene glycol) (hydroxy-(polyethyleneoxy)propyl] triethoxysilane, PEG-Si, MW = 575–750 g/mol) was incorporated into the reaction mixture in order to avoid self-aggregation in the reaction media. Finally, 3-[tris(trimethylsiloxy)silyl]propyl methacrylate (MPS) was added to provide polymerizable groups on the particle surface. Passivation with PEG helps to maintain the nanoparticle dispersity and long-term stability in various biological media and phosphate buffered saline (PBS).[25] At this point, a distribution of 78-nm magnetic mesoporous nanoparticles was obtained by dynamic light scattering that was also confirmed by SEM and TEM images (Figure S2). The organic content of the particles was determined by thermogravimetric analysis (TGA) having a 10% weight loss (Figure S3), corresponding to PEG and methacrylate groups on the silica surface. This was also confirmed by the FTIR spectra of the material that exhibited the characteristic ν_{as} (OC═O) ester band of the methacrylate groups at 1700 cm^{-1} and σ (CH) at 1472 cm^{-1} from both functionalizing agents (Figure S4). Textural parameters were evaluated by N_2 porosimetry showing a profile of mesoporous adsorption–desorption isotherms and surface area of 1391 $m^2{\cdot}g^{-1}$ (Figure S5 and Table S1) which confers high loading capacity for drug delivery purposes.[26]

Thermosensitive polymers based on poly-*N*-isopropylacrylamide (pNIPAm) are widely used for drug delivery applications because it can undergo a linear to globular phase transition when heated above its lower critical solution temperature (LCST), which is 32 °C,[27] and it presents good biocompatibility.[28] The stimuli-responsive behavior of pNIPAm-based polymers arises from the entropic gain produced when water molecules attached to the polymer chains by hydrogen-bonding are discharged to the aqueous phase above the lower critical solution temperature (LCST) or volume phase transition temperature (VPTT) when cross-linkers are used. This entropy change is responsible for the transition from hydrophilic to hydrophobic state. However, the LCST of pNIPAm is not suitable for drug delivery applications, as it is below the body temperature. For the purpose of this work, a thermosensitive polymer with an LCST of 42–45 °C was desired, in order to be in its swelling state (and pore-blocking) at body temperature (37 °C) and collapsed (and pore opening) when heated in temperatures between 42 and 45 °C. Therefore, we introduced hydrophilic comonomers in the pNIPAm chain to increase the polymer transition temperature, specifically *N*-hydroxymethyl acrylamide (NHMA), which increases the polymer–water interactions resulting in a LCST or VPTT enhancement. To synthesize a suitable polymer which suffers a polymer transition in the 41–43 °C temperature range, we first synthesized a library of linear polymers by radical polymerization in liquid phase using different NIPAM/NHMA monomer ratios (Figure 1).

The transition temperature of the synthesized polymers was determined by UV–vis spectrometry keeping the pH and the ionic strength fixed at 7.4 and 0.0134 M, respectively, following a procedure described in the Supporting Information. As expected, the LCST of the polymers augmented as the hydrophilic monomer ratio increased, while the LCST behavior

a)

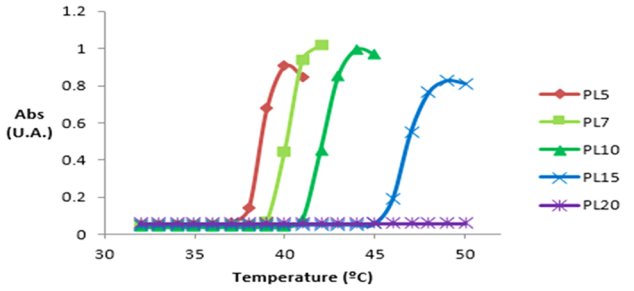

b)

Polymer	% mol monomer feed	% mol M[a] (NMR)	LCST[b] (ºC)
PL5	5	4	38
PL7	7	7	40
PL10	10	10	42
PL15	15	15	46
PL20	20	20	n.d.

[a] Determined by integration of NIPAM/NHMA signals. NHMA integrals slightly overlaps with D_2O peak (see figure S6 in the supporting information). [b] Polymer transition temperatures measured by UV-Vis spectroscopy. n.d: not detectable

Figure 1. Lower critical solution temperature changes with the increase of hydrophilic monomer NHMA for linear polymers measured by turbidimetry (a) and polymerization data obtained using 1:400 monomer-to-initiator ratio (b).

was not detectable when 20% of monomer was employed. Once we screened our prepared copolymers library, we chose for further in situ polymer attachment a feed monomer ratio of 90:10 NIPAM/NHMA, which resulted in a polymer with an LCST of 42 °C. Polymeric layer was carried out by a slight modification of the method developed by Yang et al.[29] Therefore, this NIPAM/NHMA ratio was used to coat the MMSNPs, in the presence of methylene bis(acrylamide) (MBA) for cross-linking purposes. After the polymeric shell incorporation, the MMSNPs average size distribution increased from 78 to 100 nm as measured by dynamic light scattering and in accordance with SEM and TEM images. Besides, the mesoporous structure was retained and the polymeric coating became clearly visible upon staining the nanoparticles with uranyl acetate (UA) and TEM observation following a method similar to that reported elsewere[30] (Figure 2). The amount of grafted polymer was 26% as determined by TGA (Figure S3), and FTIR demonstrated a characteristic ν_{as} (NC═O) amide band at 1650 cm^{-1} showing the grafting of the polymeric shell (Figure S4). Stability studies carried out in PBS by DLS demonstrated that the colloidal suspension was maintained for 8 h, thanks to the polymeric coating (Figure S7).

To assess the magnetically responsive behavior, the polymer-coated mesoporous nanoparticles were characterized under DC (direct current) and AC (alternating current) magnetic field conditions. DC experiments showed loops with coercive fields close to zero and saturation magnetization values of 2.80 emu·g^{-1}, evidencing the superparamagnetic behavior of the SPIONS contained within the silica matrix (Figure S8). Different conditions were considered for AC experiments using different frequencies and field amplitudes listed in Table S2. A maximum SAR of 178.53 W·g^{-1} was registered for AC fields of 20.05 kA·

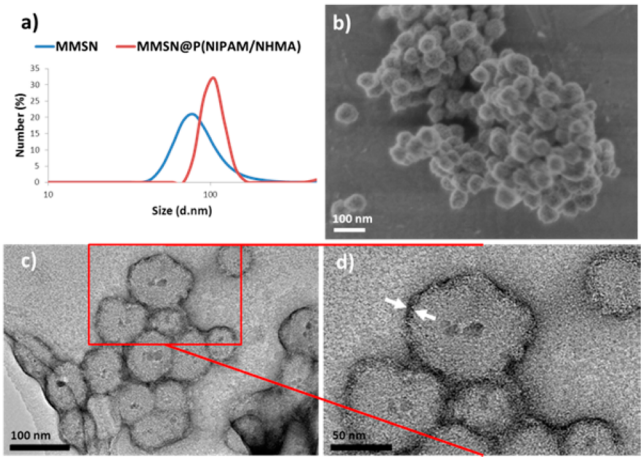

Figure 2. DLS measurements of MMSNPs and MMSNP@P(NIPAM/NHMA) (a). SEM micrographs (b) and TEM images (c) of the polymer-coated nanoparticles. Polymeric coating detail (d).

m^{-1} and 838 kHz. Therefore, these AC field parameters were selected for further experiments.

The addition of MBA as a cross-linker to obtain a dense polymer network, besides the surface coating process, could affect the polymer transition temperature of the nanodevice. Additionally, the attachment of a polymer onto a nanoparticle could affect its temperature-responsive behavior. However, LCST measurements in the presence of MMSNP were not possible, due to the UV light scattering of the nanoparticles. To confirm that the transition temperature of the polymer coating is maintained after immobilization on the surface, a colloidal suspension of 10 mg/mL fluorescein-loaded MMSNP@P(NIPAM/NHMA) nanoparticles was placed in an incubator. The target temperatures were chosen to be 37, 40, and 43 °C. After reaching the target temperatures, the samples were collected and the fluorescence of the supernatants (released fluorescein) was measured. The amounts of released fluorophore were similar at 37 and 40 °C, but once the global temperature reached 43 °C, an increase in fluorescein release was clearly observed (Figure 3). This fact indicates that the thermosensible polymer coating has its VPTT near LCST linear polymer behavior and transition temperature, being able

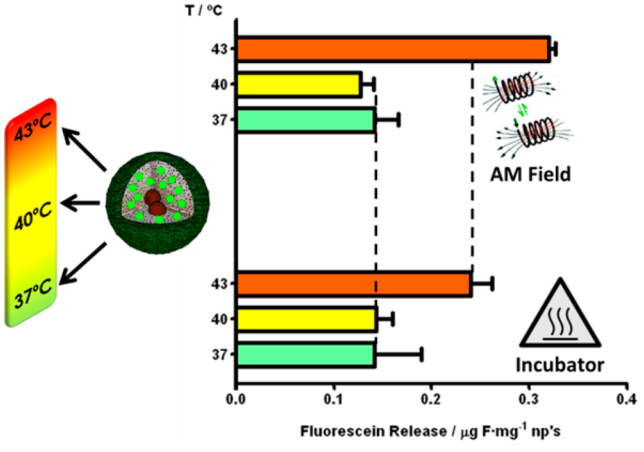

Figure 3. Fluorescein release of polymer-coated nanoparticles at different target temperatures in an incubator (top) and under AMF application (bottom).

to retain its cargo at physiological temperature and release it once the temperature overcomes the VPTT value, even with a highly soluble model drug as the fluorescein sodium salt. Time evolution of the fluorescein release was also tested at 37 and 50 °C, showing a low premature release of 20% of the cargo within the first 24 h (Figure S9). This result indicates that this device would release most of its cargo once the target tissue was reached and AMF will be applied.

Therefore, the same experiment was repeated by exposing the fluorescein-loaded particles to an AMF at a frequency of 838 kHz and a field of 20.05 $kA \cdot m^{-1}$.The temperature was monitored using a fiberoptic temperature probe, and the temperature ramp was replicated to three different global temperatures of 37, 40, and 43 °C similarly to that obtained with the incubator (Figure S10). The samples submitted to an AMF presented a similar fluorescein release profile at the three target temperatures (Figure 3).

Below the polymer's VPTT, the fluorescein release was low compared to the sample that reached 43 °C, revealing that it is possible to provoke the polymer transition under an alternating magnetic field, as we have previously described.[13] Moreover, there was a significant difference in the released cargo between the samples exposed to thermal and magnetic heating after reaching the VPTT. As it is clearly shown in Figure 3, the sample exposed to magnetic field was able to release a significantly higher amount of fluorescein in the same period of time. This variance in fluorescein release could be explained by different mechanisms: (i) the polymer transition temperature is reached faster in the particle surroundings when AMF is applied, which is consistent with previously cited works,[18,19] (ii) the localized temperature at the nanoparticle proximities is higher than the global temperature, which causes a faster diffusion of the loaded molecules once the pore is opened, and (iii) the vibrations of the SPIONs when subjected to AMF can also induce a higher release as compared to simple heating in the incubator. These mechanisms could act cooperatively resulting in the enhanced fluorescein release.

The response to heat dissipation by physiological environment is a critical issue still unclear. There are doubts whether these magnetic devices are capable to overcome the heat dissipation that is observed in living tissues. To resolve this matter of concern, we developed a second experiment by applying AMF under isotherm conditions, keeping the temperature constant at 37 °C with a water recirculating system while the AMF is applied. Then, the fluorescein release experiment was performed using this isothermal setup, placing one aliquot in the AC magnetic inductor at 37 °C, while another aliquot was placed at 37 °C in an incubator as control. The alternating magnetic field was applied for 45 min. Subsequently, the samples were rapidly cooled to 4 °C to avoid fluorescein leaking, collected by centrifugation, and the fluorescence of supernatants was measured. Results showed a 2-fold fluorescein release upon an AMF application with regard to the sample placed in an incubator (Figure 4).

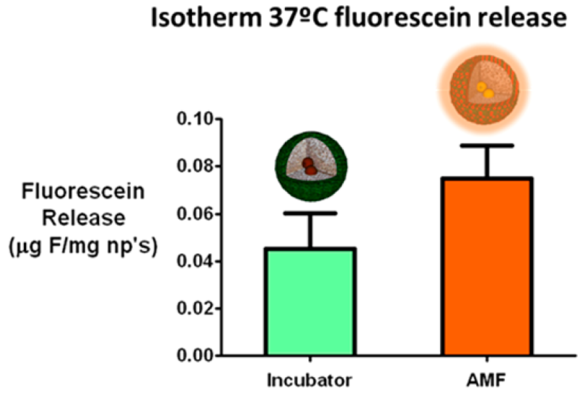

Figure 4. Fluorescein release from MMSNP@P(NIPAM/NHMA) under AMF in isothermal conditions.

CONCLUSIONS

This fact proves that thermal energy dissipated by SPIONs under a magnetic field is capable to effectively reach the surface of the nanoparticles through the silica matrix, provoking the polymer hydrophilic to hydrophobic transition and the subsequent drug release when under isothermal conditions at 37 °C, which mimics the physiological conditions. This phenomenon can be explained by the so-called *hot spot* effect, where the existence of a hot source in the interior of the device accomplishes high local temperatures but no global heating is observed.

This work shows that the application of an AMF to our system provokes the release of the cargo without the necessity to achieve a global temperature increase. The hot spots generated by magnetite nanoparticles are capable to provoke the shrinkage of the polymer network on the silica matrix, achieving the effective triggered release of the cargo. It must be highlighted that the aim of this work is not demonstrating the hot spot effect, but its capability for releasing the cargo in a stimuli-responsive way, although the environment remained at physiological temperature. Heating the environment requires much magnetic energy that, very often, is noncompatible with the clinical/technical requirements, which is a very serious limitation for the transference to the biomedical field.[31] These results pave the way to the application of magnetically triggered carriers for the treatment of complex diseases due to the biocompatibility and high penetration capacity of magnetic fields. Moreover, the presence of magnetic cores within the silica matrix opens the possibility to combine the stimuli-responsive capacity with imaging applications in the same carrier, converting this device in an excellent prototype in the theranostics field. Further work is ongoing in order to test the capacity of this device to transport and release cytotoxic drugs using in vivo models.

ASSOCIATED CONTENT

Supporting Information

The Supporting Information is available free of charge on the ACS Publications website :

Characterization techniques such as transmission and scanning electron microscopy, dynamic light scattering, nitrogen sorption isotherms, IR and NMR spectroscopy, release experiments, thermogravimetric analysis, vibrating sample magnetometer, and SAR measurements. Figures S1−S10 and Tables S1 and S2. Materials and methods used for the preparation of the nanoparticles (PDF)

AUTHOR INFORMATION

Corresponding Author

* E-mail: vallet@ucm.es; phone: 34 91 3941870; fax: 34 91 3941786.

Author Contributions

The manuscript was written through contributions of all authors. All authors have given approval to the final version of the manuscript.

Notes

The authors declare no competing financial interest.

■ ACKNOWLEDGMENTS

This work was supported by the Ministerio de Economía y Competitividad, through projects MAT2012-35556, MAT2013-43299R, and CSO2010-11384-E (Agening Network of Excellence), ERC-Starting Grant 239931-NANOPUZZLE project, and Fondo Social Europeo (FSE; Gobierno de Aragón). CIBER-BBN is an initiative funded by the VI National R&D&i Plan 2008-2011, Iniciativa Ingenio 2010, Consolider Program, CIBER Actions, and financed by the Instituto de Salud Carlos III with assistance from the European Regional Development Fund. We also thank the X-ray Diffraction C.A.I., NMR C.A.I., and the National Electron Microscopy Center, UCM. E.G. thanks CEI Campus Moncloa for the PICATA fellowship.

■ REFERENCES

(1) Jain, R. K.; Stylianopoulos, T. Delivering Nanomedicine to Solid Tumors. *Nat. Rev. Clin. Oncol.* **2010**, *7*, 653−664.
(2) Baeza, A.; Colilla, M.; Vallet-Regí, M. Advances in Mesoporous Silica Nanoparticles for Targeted Stimuli-Responsive Drug Delivery. *Expert Opin. Drug Delivery* **2015**, *12*, 319−337.
(3) Vallet-Regi, M.; Rámila, a.; Del Real, R. P.; Pérez-Pariente, J. A New Property of MCM-41: Drug Delivery System. *Chem. Mater.* **2001**, *13*, 308−311.
(4) Maeda, H.; Nakamura, H.; Fang, J. The EPR Effect for Macromolecular Drug Delivery to Solid Tumors: Improvement of Tumor Uptake, Lowering of Systemic Toxicity, and Distinct Tumor Imaging in Vivo. *Adv. Drug Delivery Rev.* **2013**, *65*, 71−79.
(5) Wicki, A.; Witzigmann, D.; Balasubramanian, V.; Huwyler, J. Nanomedicine in Cancer Therapy: Challenges, Opportunities, and Clinical Applications. *J. Controlled Release* **2015**, *200*, 138−157.
(6) Angelos, S.; Khashab, N. M.; Yang, Y. W.; Trabolsi, A.; Khatib, H. a.; Stoddart, J. F.; Zink, J. I. pH Clock-Operated Mechanized Nanoparticles. *J. Am. Chem. Soc.* **2009**, *131*, 12912−12914.
(7) Chen, L.; Li, L.; Zhang, L.; Xing, S.; Wang, T.; Wang, Y. A.; Wang, C.; Su, Z. Designed Fabrication of Unique Eccentric Mesoporous Silica Nanocluster-Based Core-Shell Nanostructures for pH-Responsive Drug Delivery. *ACS Appl. Mater. Interfaces* **2013**, *5*, 7282−7290.
(8) Mackowiak, S. A.; Schmidt, A.; Weiss, V.; Argyo, C.; von Schirnding, C.; Bein, T.; Brauchle, C. Targeted Drug Delivery in Cancer Cells with Red Light Photoactivated Mesoporous Silica Nanoparticles. *Nano Lett.* **2013**, *13*, 2576−2583.
(9) Zhang, J.; Yuan, Z. F.; Wang, Y.; Chen, W. H.; Luo, G. F.; Cheng, S. X.; Zhuo, R. X.; Zhang, X. Z. Multifunctional Envelope-Type Mesoporous Silica Nanoparticles for Tumor-Triggered Targeting Drug Delivery. *J. Am. Chem. Soc.* **2013**, *135*, 5068−5073.
(10) Slowing, I. I.; Trewyn, B. G.; Giri, S.; Lin, V. S. Y. Mesoporous Silica Nanoparticles for Drug Delivery and Biosensing Applications. *Adv. Funct. Mater.* **2007**, *17*, 1225−1236.
(11) Tarn, D.; Ashley, C. E.; Xue, M.; Carnes, E. C.; Zink, J. I.; Brinker, C. J. Mesoporous Silica Nanoparticle Nanocarriers: Biofunctionality and Biocompatibility. *Acc. Chem. Res.* **2013**, *46*, 792−801.
(12) Ruiz-Hernández, E.; Baeza, A.; Vallet-Regí, M. Smart Drug Delivery through DNA/Magnetic Nanoparticle Gates. *ACS Nano* **2011**, *5*, 1259−1266.
(13) Baeza, A.; Guisasola, E.; Ruiz-Hernández, E.; Vallet-Regí, M. Magnetically Triggered Multidrug Release by Hybrid Mesoporous Silica Nanoparticles. *Chem. Mater.* **2012**, *24*, 517−524.
(14) Chang, B.; Sha, X.; Guo, J.; Jiao, Y.; Wang, C.; Yang, W. Thermo and pH Dual Responsive, Polymer Shell Coated, Magnetic Mesoporous Silica Nanoparticles for Controlled Drug Release. *J. Mater. Chem.* **2011**, *21*, 9239.
(15) Liu, C.; Guo, J.; Yang, W.; Hu, J.; Wang, C.; Fu, S. Magnetic Mesoporous Silica Microspheres with Thermo-Sensitive Polymer Shell for Controlled Drug Release. *J. Mater. Chem.* **2009**, *19*, 4764.
(16) Wust, P.; Hildebrandt, B.; Sreenivasa, G.; Rau, B.; Gellermann, J.; Riess, H.; Felix, R.; Schlag, P. M. Hyperthermia in Combined Treatment of Cancer. *Lancet Oncol.* **2002**, *3*, 487−497.
(17) Dutz, S.; Hergt, R. Magnetic Nanoparticle Heating and Heat Transfer on a Microscale: Basic Principles, Realities and Physical Limitations of Hyperthermia for Tumour Therapy. *Int. J. Hyperthermia* **2013**, *29*, 790−800.
(18) Dias, J. T.; Moros, M.; Del Pino, P.; Rivera, S.; Grazú, V.; de la Fuente, J. M. DNA as a Molecular Local Thermal Probe for the Analysis of Magnetic Hyperthermia. *Angew. Chem., Int. Ed.* **2013**, *52*, 11526−11529.
(19) Riedinger, A.; Guardia, P.; Curcio, A.; Garcia, M. A.; Cingolani, R.; Manna, L.; Pellegrino, T. Subnanometer Local Temperature Probing and Remotely Controlled Drug Release Based on Azo-Functionalized Iron Oxide Nanoparticles. *Nano Lett.* **2013**, *13*, 2399−2406.
(20) Dong, J.; Zink, J. I. Taking the Temperature of the Interiors of Magnetically Heated Nanoparticles. *ACS Nano* **2014**, *8*, 5199−5207.
(21) Kim, J.; Kim, H. S.; Lee, N.; Kim, T.; Yu, T.; Song, I. C.; Moon, W. K.; Hyeon, T.; Kim, H. Multifunctional Uniform Nanoparticles Composed of a Magnetite Nanocrystal Core and a Mesoporous Silica Shell for Magnetic Resonance and Fluorescence Imaging and for Drug Delivery. *Angew. Chem.* **2008**, *120*, 8566−8569.
(22) Lin, Y.-S.; Hurley, K. R.; Haynes, C. L. Critical Considerations in the Biomedical Use of Mesoporous Silica Nanoparticles. *J. Phys. Chem. Lett.* **2012**, *3*, 364−374.
(23) Meng, H.; Xue, M.; Xia, T.; Ji, Z.; Tarn, D. Y.; Zink, J. I.; Nel, A. E. Use of Size and a Copolymer Design Feature to Improve the Biodistribution and the Enhanced Permeability and Retention Effect of Doxorubicin-Loaded Mesoporous Silica Nanoparticles in a Murine Xenograft Tumor Model. *ACS Nano* **2011**, *5*, 4131−4144.
(24) Lin, Y.-S. S.; Haynes, C. L. Synthesis and Characterization of Biocompatible and Size-Tunable Multifunctional Porous Silica Nanoparticles. *Chem. Mater.* **2009**, *21*, 3979−3986.
(25) Lin, Y.-S.; Abadeer, N.; Haynes, C. L. Stability of Small Mesoporous Silica Nanoparticles in Biological Media. *Chem. Commun.* **2011**, *47*, 532−534.
(26) Vallet-Regí, M.; Balas, F.; Arcos, D. Mesoporous Materials for Drug Delivery. *Angew. Chem., Int. Ed.* **2007**, *46*, 7548−7558.
(27) Schild, H. G. Poly (N-Isopropylacrylamide): Experiment, Theory and Application. *Prog. Polym. Sci.* **1992**, *17*, 163−249.
(28) Wadajkar, A. S.; Koppolu, B.; Rahimi, M.; Nguyen, K. T. Cytotoxic Evaluation of N-Isopropylacrylamide Monomers and Temperature-Sensitive poly(N-Isopropylacrylamide) Nanoparticles. *J. Nanopart. Res.* **2009**, *11*, 1375−1382.
(29) Chang, B.; Chen, D.; Wang, Y.; Chen, Y.; Jiao, Y.; Sha, X.; Yang, W. Bioresponsive Controlled Drug Release Based on Mesoporous Silica Nanoparticles Coated with Reductively Sheddable Polymer Shell. *Chem. Mater.* **2013**, *25*, 574−585.
(30) Baeza, A.; Guisasola, E.; Torres-Pardo, A.; González-Calbet, J. M.; Melen, G. J.; Ramirez, M.; Vallet-Regí, M. Hybrid Enzyme-Polymeric Capsules/mesoporous Silica Nanodevice for in Situ Cytotoxic Agent Generation. *Adv. Funct. Mater.* **2014**, *24*, 4625−4633.
(31) Brezovich, I. A.; Meredith, R. F. Practical Aspects of Ferromagnetic Thermoseed Hyperthermia. *Radiol. Clin. North Am.* **1989**, *27*, 589−602.